NANO LETTERS

Letter

pubs.acs.org/NanoLett

Superresolution Microscopy with Quantum Emitters

Osip Schwartz,* Jonathan M. Levitt, Ron Tenne, Stella Itzhakov, Zvicka Deutsch, and Dan Oron

Department of Physics of Complex Systems, Weizmann Institute of Science, Rehovot, Israel, 76100

Supporting Information

ABSTRACT: The optical diffraction limit imposes a bound on imaging resolution in classical optics. Over the last twenty years, many theoretical schemes have been presented for overcoming the diffraction barrier in optical imaging using quantum properties of light. Here, we demonstrate a quantum superresolution imaging method taking advantage of nonclassical light naturally produced in fluorescence microscopy due to photon antibunching, a fundamentally quantum phenomenon inhibiting simultaneous emission of multiple photons. Using a photon counting digital camera, we detect antibunching-induced second and third order intensity correlations and perform subdiffraction limited quantum imaging in a standard wide-field fluorescence microscope.

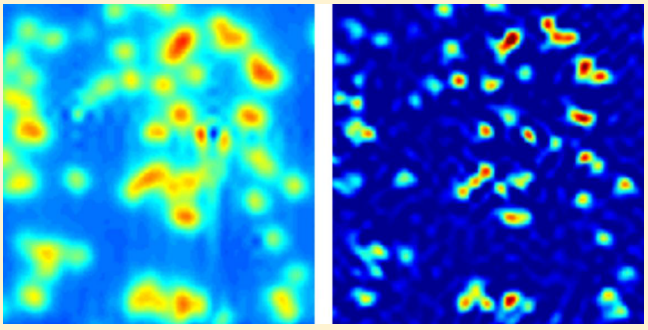

KEYWORDS: *Superresolution, optical microscopy, photon antibunching, quantum imaging, quantum dots*

The optical diffraction limit restricts the resolution of far-field optical microscopes to approximately half the wavelength of light. Abbe's description of the imaging system[1] is based on the laws of classical linear optics, applied to stationary objects. Correspondingly, there are three loopholes in the argument, concerning the linearity, stationarity, and classicality assumptions. In the last two decades, superresolution imaging methods were developed based on nonlinear optical effects such as stimulated emission,[2] optical shelving[3] and fluorescence saturation.[4,5] More recently, subdiffraction limited imaging was achieved by another class of microscopy methods, making use of nonstationary emission of fluorescent markers caused either by photoswitching,[6,7] or by intrinsic brightness fluctuations.[8,9]

The remaining loophole for overcoming the diffraction barrier, resorting to quantum optics, has received a lot of attention in the recent years. It has been shown that high order quantum interference patterns arising in quantum optics can yield spatial distribution of correlations much tighter than classically allowed. Such fringes have been observed using coincidence detection in various settings.[10−12] It seems tempting to use these sharp spatial features to image subwavelength details of microscopic objects. Several quantum superresolution schemes have been proposed, utilizing multimode squeezed light,[13] an arrangement of single photon emitters,[14] or generalized quantum states of light.[15−17] At the same time, although quantum optical methods have enabled image entanglement[18] and subshot noise imaging,[19] as well as quantum optical coherence tomography with improved depth resolution,[20] subdiffraction limited quantum imaging has not yet been experimentally demonstrated.

The common element of most proposed quantum superresolution schemes is illuminating an absorptive sample with a nonclassical state of light. An alternative approach, proposed theoretically by Hell et al.,[21] relies on nonclassical properties of light emitted by the sample itself, while using regular laser light for illumination. It was shown in this work that a hypothetical quantum emitter producing photons only in pairs (or groups) can be imaged using coincidence detection with a resolution increase similar to that attainable in two-photon (multiphoton) microscopy. Unfortunately, the technique has not been taken up experimentally since no suitable multiphoton emitting fluorophore has ever been introduced.

Here, we extend the idea of multiphoton detection put forward by Hell et al.[21] by utilizing fluorophores in which emission of more than one photon is suppressed. This phenomenon, known as photon antibunching,[22] is observed in most common fluorophores, such as organic dyes[23] or quantum dots,[24,25] even under ambient conditions. The necessary quantum emitters are thus widely used in fluorescence microscopy, a ubiquitous life science imaging tool. Because of photon antibunching, in every point of the image plane of a fluorescence microscope photon statistics is sub-Poissonian,[26] that is, the number of simultaneous multiphoton detection events is smaller in every order than it is for classical light. Quantifying the missing N-photon coincidence events gives a signal equivalent to N-photon detection signal, narrowing the effective point spread function by a factor of $\sqrt{N}$.[27] In this work, we detect photon statistics in the image plane of a wide-field fluorescence microscope, determine the spatial distribution of missing two- and three-photon

Received: July 11, 2013
Revised: October 8, 2013
Published: November 6, 2013

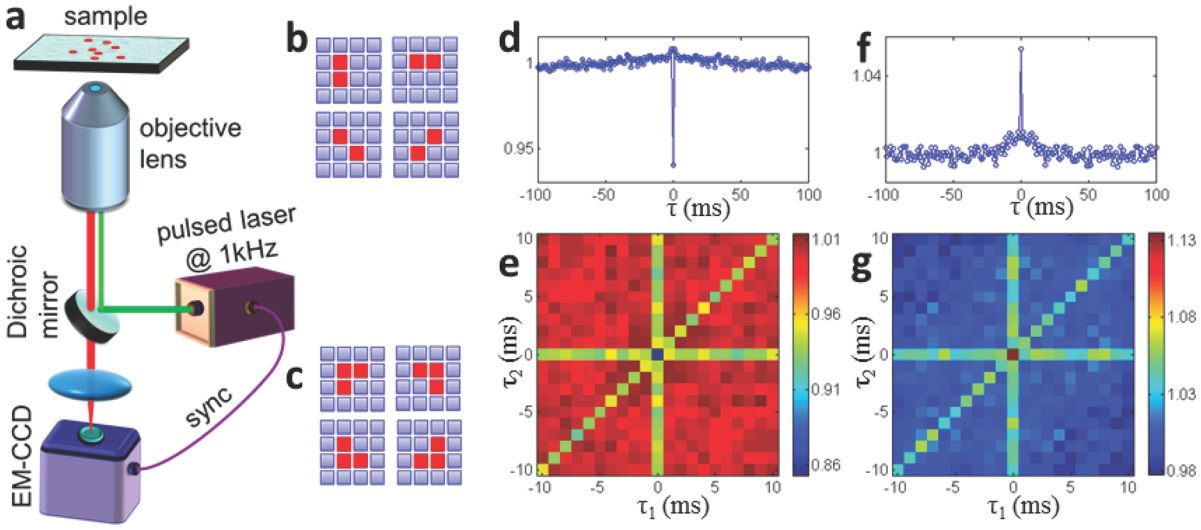

Figure 1. Detecting nonclassical correlations in fluorescence microscopy. (a) A schematic of the experimental setup used for correlation imaging. (b,c) The pixel configurations used for second and third order correlation detection, respectively. (d) A typical second order intensity correlation function from an eight-pixel region on the CCD covering an image of a single emitter, computed as $g^{(2)}(\tau) = \sum_{i\neq k}[\langle n_i(t)n_k(t+\tau)\rangle]/[\langle n_i\rangle\langle n_k\rangle]$, where the sum runs over all pixel pairs in the relevant region and angle brackets indicate averaging over t. The graph features an antibunching dip. Panel (e) demonstrates a two-dimensional plot representing third order autocorrelation $g^{(3)}(\tau_1,\tau_2) = \sum[\langle n_i(t)n_k(t+\tau_1)n_m(t+\tau_2)\rangle]/(\langle n_i\rangle\langle n_k\rangle\langle n_m\rangle)$, where the sum runs over all three-pixel combinations within the same region of interest. (f) A correlation function computed for the same region on the CCD illuminated with a classical light source with a bunching peak at zero delay. (g) The third order correlation measured with classical signal demonstrates behavior opposite to antibunching: it has ridges at $\tau_1 = 0$, at $\tau_2 = 0$, and at $\tau_1 = \tau_2$ and a peak at $\tau_1 = \tau_2 = 0$.

coincidence events, and reconstruct second and third order superresolved images.

Our measurement scheme relies on detecting fluorescence intensity correlations. Classically, when fluorescent light impinges on an array of independent photodetectors, their signals are uncorrelated (assuming that Hanbury Brown−Twiss type correlations are negligible, which is the case in our experimets, see Supporting Information for details). In contrast, when a perfectly antibunched emitter is imaged onto a detector array, the single photon it emits following excitation can arrive to only one of the detectors. Antibunching thus creates negative correlations between independent detectors. We define the second order antibunching signal as unnormalized second order correlation function $A^{(2)}(x) = I^2(x)(1-g^{(2)}(x,0))$, where $g^{(2)}(x,\tau)$ is the second order Glauber coherence function measured at the point x with the delay τ, and $I(x)$ is the mean fluorescence intensity at the same point. Higher order antibunching signals can be similarly defined as N-point irreducible intensity correlation functions. Importantly, contributions to the antibunching signal from individual fluorophores are additive and can therefore be utilized as a local measure of the emitter density thus directly providing superresolved images of the fluorophore spatial distribution.[27]

For the proof of principle demonstration of antibunching imaging, we used test samples consisting of CdSe/CdS/ZnS colloidal quantum dots (QDs), commonly used as labels in fluorescence microscopy,[28] with the main emission peak at 617 nm. The QDs were embedded in a thin polymer film spin-coated onto a glass slide (see Supporting Information for further details). Such QDs demonstrate pronounced photon antibunching[24] due to strong charge carrier interactions leading to rapid nonradiative relaxation in multiply excited QDs.[29]

Experimental observation of nonclassical intensity correlations was carried out using a regular wide-field epi-fluorescence microscope shown schematically in Figure 1a. To detect photon statistics simultaneously in the entire field of view, we used an electron multiplying charge-coupled device (EM-CCD) in the photon counting mode as a fluorescence detector. The fluorophores were excited with 300 ps laser pulses at 532 nm, with pulse energy sufficient to optically saturate the QDs. Following emitter relaxation, the image was read out and stored in a computer. The excitation pulse/image readout sequence was repeated at a rate of 1 kHz. The pixel readings were thresholded to produce maps of photon detection events, while the probability of detecting more than one photon per pixel in the same excitation cycle was negligible.

Gathering sufficient photon statistics for superresolution imaging requires a high probability of photon detection from an individual emitter in every excitation cycle. Although near-unity detection efficiency has been achieved with emitters embedded in specially designed dielectric structures[30] in regular fluorescent microscopy the fluorophores usually operate well below saturation to avoid photobleaching. However, at the repetition rate as low as 1 kHz QDs exhibit nearly absolute photostability and can be saturated indefinitely without inflicting photodamage.[31] This enabled detection rates of about 0.1 photon per emitter per excitation cycle, which proved sufficient to detect the antibunching-induced correlations in the image plane.

First, we set out to confirm that photon antibunching can be observed in our setup by measuring $g^{(2)}(\tau)$. This correlation function is commonly detected using a pair of single photon detectors in a Hanbury Brown−Twiss configuration and computed as the normalized coincidence probability.[23,24] We adopted this standard measurement procedure by using a pair of adjacent EM-CCD pixels instead of single photon detectors. The temporal resolution of detection was naturally limited to one CCD frame duration, confining our measurement of $g^{(2)}(\tau)$ to discrete times. The second order coherence function was computed as $g^{(2)}_{ik}(\tau) = [\langle n_i(t)n_k(t+\tau)\rangle]/[\langle n_i\rangle\langle n_k\rangle]$, where $n_i(t)$ and $n_k(t+\tau)$ are the numbers of photons (either zero or one) detected in pixels i and k at frames t and $t+\tau$, respectively, and

dx.doi.org/10.1021/nl402552m | Nano Lett. 2013, 13, 5832−5836

the angle brackets denote averaging over t. To improve the signal-to-noise ratio, the resulting correlation function was averaged over several distinct pixel pairs within a small region of the CCD.

A typical correlation function shown in Figure 1d exhibits the characteristic antibunching dip at zero delay. Furthermore, we were able to detect antibunching features in the third order intensity correlation function $g^{(3)}_{ikm}(\tau_1,\tau_2) = [\langle n_i(t)n_k(t + \tau_1)n_m(t + \tau_2)\rangle]/[\langle n_i\rangle\langle n_k\rangle\langle n_m\rangle]$, depending on two discrete delay times τ_1 and τ_2. A two-dimensional plot of a typical third order temporal correlation function is shown in Figure 1e. The plot features depressed lines at $\tau_1 = 0$, at $\tau_2 = 0$, and at $\tau_1 = \tau_2$, which represent the lack of two-photon coincidence events. The central data point of this plot, at $\tau_1 = \tau_2 = 0$, which is depressed even further, corresponds to the missing three-photon coincidence events. The dips in the correlation functions represent the nonclassical signal that we proceed to utilize to produce superresolved images. The observed magnitude of the antibunching features is reduced due to frame-to-frame fluctuations in the CCD readout circuitry, leading to apparent bunching of detection events. Our data processing offsets the antibunching signal to account for this effect.

To quantify the second order antibunching signal at every point in the image plane with subdiffraction limited resolution, we computed the cross-correlations between pairs of neighboring pixels in configurations shown in Figure 1b. The resulting four correlation maps were Fourier-interpolated and summed. Similarly, the third order antibunching images were obtained by computing the third order cross-correlation for pixel configurations shown in Figure 1c. The details of the data processing are described in the Supporting Information.

A typical superresolved image set is shown in Figure 2. A regular fluorescence image and the second and third order antibunching images of the same area, presented in Figure 2a–c, demonstrate consecutive improvement of resolution. The magnified view of a small region (Figure 2d–f) illustrates the initially unresolved features of QD distribution revealed by antibunching imaging. Enhanced resolution is also evident in the line scan plotted in Figure 2g. Quantitatively, the resolution defined as the full width at half-maximum of the point spread function improves from 272 nm in regular images to 216 nm in the second order and 181 nm in the third order, corresponding to a resolution enhancement by a factor of 1.5 (see Supporting Information for resolution quantification and additional antibunching images).

In addition to improving the transverse resolution, antibunching imaging has an optical sectioning capability similar to that demonstrated by multiphoton excitation microscopy. This is illustrated by the out-of-focus images of a QD presented in Figure 3. A comparison of the regular fluorescent images of Figure 3a with the corresponding second order antibunching images shown in Figure 3b demonstrates that the antibunching signal decreases faster with defocusing than regular fluorescence. While the regular fluorescence signal is blurred by defocusing, in transparent medium its integral remains unchanged, leading to out-of-focus background in wide-field microscopy. In contrast, the second order antibunching signal fades away with defocusing, leading to discrimination of the out-of-focus signal. Figure 3c shows variation of the total signal, integrated over the field of view, as a function of defocusing for regular fluorescence imaging and for the second order antibunching signal.

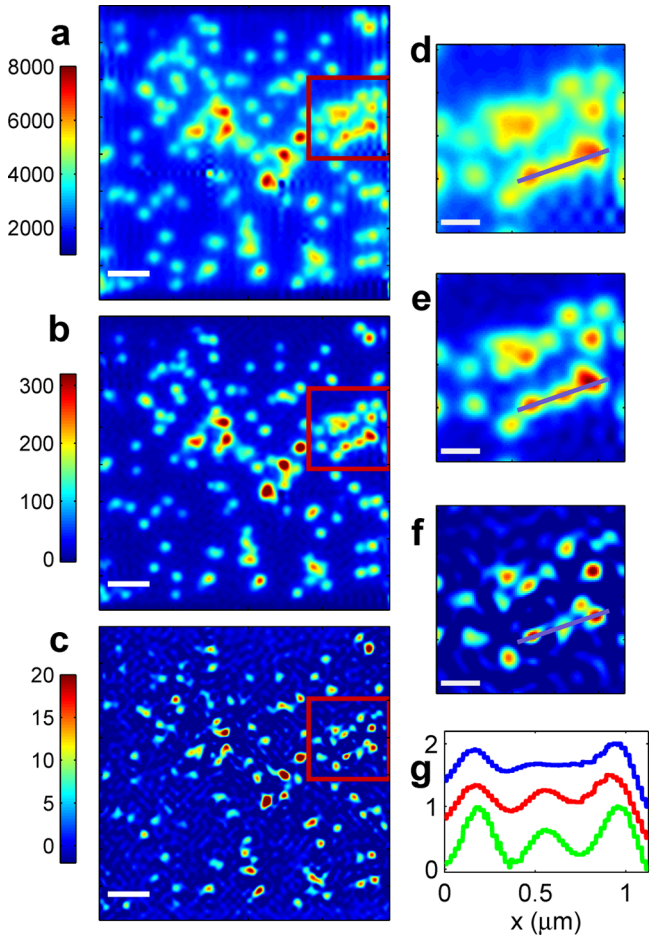

Figure 2. Fluorescence antibunching imaging. Panels (a–c) show a regular fluorescence image, second, and third order antibunching images, respectively. Scalebar length is 1 μm. (d–f) Magnified views of the boxed areas in the images (a–c). Scalebar is 400 nm. The graph presented in panel (g) shows a cut of the magnified images (in normalized units) along the line indicated in panels (d–f). The blue line corresponds to regular fluorescence image and the red and green lines represent the second and third order antibunching imaging, respectively. The lines are vertically shifted for visibility.

Whereas photon antibunching is undoubtedly a quantum phenomenon that cannot be interpreted in terms of classical electrodynamics,[32,33] it is important to discuss to what extent the resolution improvement in antibunching imaging can be attributed to quantum properties of light. To this end, we note that antibunching imaging can be applied to a static object consisting of ideal two-level quantum scatterers with no time-dependent properties. In this case, fluorescent light would be in a well-defined quantum state, reproduced identically in every excitation cycle. The high spatial frequency information would then be revealed by antibunching imaging in the process of statistical characterization of that state. It is clear, however, that this can only be possible if the superresolution information is imprinted in the quantum state of light radiated by the fluorophores. Considering that classically no information beyond the diffraction limit can be carried by light, we conclude that, indeed, it is the quantum properties of fluorescent light that enable breaking the Abbe limit in antibunching microscopy.

The antibunching based superresolution imaging method presented here is closely related to Superresolution Optical

dx.doi.org/10.1021/nl402552m | Nano Lett. 2013, 13, 5832–5836

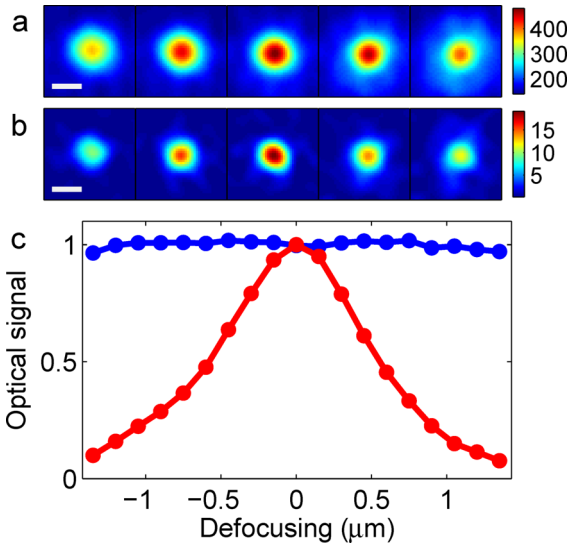

Figure 3. Regular fluorescence and second order antibunching imaging dependence on defocusing. Panels (a) and (b) show, respectively, regular fluorescence and second order antibunching images of a QD with the imaging system focused (left to right) at −880, −440, 0, 440, and 740 nm relative to the sample. Scale bar is 250 nm. Panel (c) shows the total signal integrated over the field of view, as a function of defocusing. The blue line represents regular fluorescence. The red line corresponds to second order antibunching imaging. The integrated fluorescence signal is practically constant as a function of depth. In contrast, the integrated antibunching signal decays quickly with defocusing.

Fluctuation Imaging (SOFI).[9] In both approaches, intensity correlations are detected in the image plane of a fluorescence microscope. The main difference between the two is the source of the signal fluctuations: fluorophore brightness fluctuations leading to super-Poissonian photon statistics in SOFI, and antibunched emission resulting in sub-Poissonian statistics in antibunching microscopy. Correspondingly, SOFI signal is highly dependent on the character of emission fluctuations exhibited by the fluorophores, which varies widely from one species to another,[34] while in antibunching imaging the statistical properties of signal giving rise to the superresolved images are universal, arising from steady emission of fluorophores with no fluctuations other than antibunching-modified shot noise.

Performance of antibunching imaging is limited at present by the parameters of the camera used for photon detection. The rapid progress of the photon detector technologies in the recent years gives hope that fast and low-noise detectors will become available in the near future, which will dramatically improve the practical prospects of antibunching imaging.

In summary, we have demonstrated a superresolution imaging technique enabled by the quantum properties of light inherent in fluorescence microscopy, bringing quantum imaging a step closer to practical applications.

■ ASSOCIATED CONTENT

Supporting Information

QD synthesis and sample preparation. Experimental setup details. The role of classical intensity correlations. A comprehensive description of the data processing procedure. Imaging resolution quantification. This material is available free of charge via the Internet at http://pubs.acs.org.

■ AUTHOR INFORMATION

Corresponding Author

*E-mail: osip.schwarz@weizmann.ac.il.

Notes

The authors declare no competing financial interest.

■ ACKNOWLEDGMENTS

Financial support by the European Research Council Starting Investigator Grant SINSLIM 258221 and by the Crown center of photonics is gratefully acknowledged. O.S. is supported by the Adams Fellowship Program of the Israel Academy of Sciences and Humanities. D.O. is the incumbent of the Recanati career development chair in energy research.

■ REFERENCES

(1) Abbe, E. *Arch. Mikrosk. Anat.* **1873**, *9*, 413.
(2) Hell, S. W.; Wichmann, J. *Opt. Lett.* **1994**, *19*, 780−782.
(3) Hell, S. W..; Dyba, M.; Jakobs, S. *Curr. Opin. Neurobiol.* **2004**, *14*, 599−609.
(4) Heintzmann, R.; Jovin, T. M.; Cremer, C. *J. Opt. Soc. Am. A* **2002**, *19*, 1599−1609.
(5) Gustafsson, M. G. L. *Proc. Nat. Acad. Sci. U.S.A.* **2005**, *102*, 13081−13086.
(6) Betzig, E.; Patterson, G.; Sougrat, R.; Lindwasser, O.; Olenych, S.; Bonifacino, J.; Davidson, M.; Lippincott-Schwartz, J.; Hess, H. *Science* **2006**, *313*, 1642.
(7) Rust, M. J.; Bates, M.; Zhuang, X. *Nat. Methods* **2006**, *3*, 793−796.
(8) Lidke, K.; Rieger, B.; Jovin, T.; Heintzmann, R. *Opt. Express* **2005**, *13*, 7052−7062.
(9) Dertinger, T.; Colyer, R.; Iyer, G.; Weiss, S.; Enderlein, J. *Proc. Nat. Acad. Sci. U.S.A.* **2009**, *106*, 22287.
(10) Walther, P.; Pan, J.; Aspelmeyer, M.; Ursin, R.; Gasparoni, S.; Zeilinger, A. *Nature* **2004**, *429*, 158−161.
(11) Afek, I.; Ambar, O.; Silberberg, Y. *Science* **2010**, *328*, 879.
(12) Shin, H.; Chan, K.; Chang, H.; Boyd, R. *Phys. Rev. Lett.* **2011**, *107*, 83603.
(13) Kolobov, M. I.; Fabre, C. *Phys. Rev. Lett.* **2000**, *85*, 3789−3792.
(14) Thiel, C.; Bastin, T.; Martin, J.; Solano, E.; Von Zanthier, J.; Agarwal, G. *Phys. Rev. Lett.* **2007**, *99*, 133603.
(15) Saleh, B.; Teich, M.; Sergienko, A. *Phys. Rev. Lett.* **2005**, *94*, 223601.
(16) Tsang, M. *Phys. Rev. Lett.* **2009**, *102*, 253601.
(17) Giovannetti, V.; Lloyd, S.; Maccone, L.; Shapiro, J. *Phys. Rev. A* **2009**, *79*, 013827.
(18) Boyer, V.; Marino, A. M.; Pooser, R. C.; Lett, P. D. *Science* **2008**, *321*, 544−547.
(19) Brida, G.; Genovese, M.; Berchera, I. *Nat. Photonics* **2010**, *4*, 227−230.
(20) Nasr, M. B.; Saleh, B. E. A.; Sergienko, A. V.; Teich, M. C. *Phys. Rev. Lett.* **2003**, *91*, 083601.
(21) Hell, S. W.; Soukka, J.; Hänninen, P. *Bioimaging* **1995**, *3*, 64−69.
(22) Kimble, H. J.; Dagenais, M.; Mandel, L. *Phys. Rev. Lett.* **1977**, *39*, 691−695.
(23) Basché, T.; Moerner, W.; Orrit, M.; Talon, H. *Phys. Rev. Lett.* **1992**, *69*, 1516−1519.
(24) Lounis, B.; Bechtel, H.; Gerion, D.; Alivisatos, P.; Moerner, W. *Chem. Phys. Lett.* **2000**, *329*, 399−404.
(25) Michler, P.; Imamoglu, A.; Mason, M.; Carson, P.; Strouse, G.; Buratto, S. *Nature* **2000**, *406*, 968−970.
(26) Mandel, L. *Opt. Lett.* **1979**, *4*, 205−207.
(27) Schwartz, O.; Oron, D. *Phys. Rev. A* **2012**, *85*, 33812.
(28) Michalet, X.; Pinaud, F.; Bentolila, L.; Tsay, J.; Doose, S.; Li, J.; Sundaresan, G.; Wu, A.; Gambhir, S.; Weiss, S. *Science* **2005**, *307*, 538−544.
(29) Jha, P. P.; Guyot-Sionnest, P. *ACS Nano* **2009**, *3*, 1011−1015.

(30) Lee, K.; Chen, X.; Eghlidi, H.; Kukura, P.; Lettow, R.; Renn, A.; Sandoghdar, V.; Götzinger, S. *Nat. Photonics* **2011**, *5*, 166−169.
(31) Schwartz, O.; Tenne, R.; Levitt, J.; Deutsch, Z.; Itzhakov, S.; Oron, D. *ACS Nano* **2012**, *6* (10), 8778−8782.
(32) Paul, H. *Rev. Mod. Phys.* **1982**, *54*, 1061.
(33) Mandel, L. *Phys. Scr.* **1986**, *1986*, 34.
(34) Cichos, F.; von Borczyskowski, C.; Orrit, M. *Curr. Opin. Colloid Interface Sci.* **2007**, *12*, 272−284.

dx.doi.org/10.1021/nl402552m | *Nano Lett.* 2013, 13, 5832−5836